Simulation of Planar Entrance Flow Using Strain-Rate-Dependent Shear and Elongational Viscosities

MAHESH GUPTA
Department of Mechanical Engineering–Engineering Mechanics
Michigan Technological University
Houghton, MI 49931

ABSTRACT: A finite element simulation of the flow in a planar channel with an abrupt contraction is presented. The effect of the elongational viscosity of a polymer on the entrance flow is analyzed employing a truncated power-law model. The power-law index and the strain rate characterizing the transition from Newtonian to power-law behavior for the elongational viscosity are treated as being independent of the values of these two parameters for the shear viscosity. The effect of flow rate on planar entrance flow is also analyzed. It is confirmed that Trouton ratio is important in determining the recirculating vortex and the extra pressure loss in entrance flow. Extra pressure loss and vortex length predicted by a finite element simulation of a planar entrance loss are compared with the corresponding predictions from Binding's approximate analysis.

INTRODUCTION

DUE TO THE elongational flow near an abrupt contraction in a channel (entrance flow), in addition to the pressure drop for fully developed flow in the upstream and downstream channels, an extra pressure loss is encountered in an entrance flow. Since the long chain molecules of a polymer exhibit stiff resistance to an elongational deformation, this extra pressure loss, called entrance loss, can be particularly large for polymers. To minimize the entrance pressure loss, in a polymeric flow, large recirculating vortices are often formed near the abrupt contraction [1–7]. The formation of recirculating vortices reduces the elongation rate near the abrupt contraction, resulting in a smaller entrance pressure loss.

To simulate the entrance flow of polymers, two different constitutive theories, namely, the generalized Newtonian formulation, and viscoelastic formulation, have been extensively used in the literature. Even though, the generalized Newtonian constitutive equations can accurately predict the shear-thinning viscosity of polymers, the predicted elongational viscosity by such a formulation is generally

0731-6844/01/04 0341–15 $10.00/0 DOI: 10.1106/RCF9-1RX6-ULKV-1JGL

smaller than the actual elongational viscosity of a polymer. Therefore, the entrance loss predicted by a generalized Newtonian formulation is smaller than its experimental value [8–12]. In comparison to generalized Newtonian formulation, viscoelastic constitutive equations predict much higher elongational viscosity and hence, a larger entrance pressure loss [13–21]. However, the elongational viscosity and the entrance pressure loss predicted by a viscoelastic constitutive equation may not accurately match with the corresponding experimental values, particularly, if only the shear properties of polymer are used to estimate the rheological parameters in the constitutive equation. Moreover, most of the numerical schemes for simulation of viscoelastic flows do not converge at higher strain rates, limiting their application to simulate the flow in various polymer processing techniques.

In the present work, a software for simulation of planar polymeric flows has been developed. To simulate a polymeric flow, this software requires strain-rate dependence of shear as well as elongational viscosity. This newly developed software has been used in this paper to analyze the effect of elongational viscosity on the entrance pressure loss and formation of recirculating vortices in an entrance flow. Similar investigation for an axisymmetric entrance flow can be found in Reference [22].

SHEAR AND ELONGATIONAL VISCOSITIES IN A PLANAR FLOW

The shear and elongational viscosities of a Newtonian fluid are constant. For a planar flow of Newtonian fluids, the Trouton ratio (Tr), which is defined as the ratio of the elongational viscosity to shear viscosity, is 4. At low strain rate the shear and elongational viscosities of a polymer are typically constant with $Tr = 4$ for a planar flow. Beyond the Newtonian range, shear viscosity of a polymer decreases as the strain rate is increased, whereas the variation of elongational viscosity beyond the Newtonian range depends upon the polymer. The experimental data in the literature show that as the strain rate is increased beyond the Newtonian range, the elongational viscosity of a polymer may decrease [23–25], remain constant [26], increase initially followed by a decrease [27] or it may exhibit a more complex behavior, such as a second increase beyond the strain-thinning region [28].

As reported in Reference [22], in the present work, the shear and elongational viscosities have been represented as functions of the second invariant of the strain rate tensor $\tilde{e} = (\nabla\hat{v} + \nabla\hat{v}^T)/2$, where $\hat{v}$ is the velocity vector. The shear as well as elongational viscosities have been represented by truncated power-law model (Figure 1):

$$\eta_s = Ae_{II}^{n-1} \text{ for } e_{II} > e_0 \qquad \eta_s = \eta_0 \text{ for } e_{II} \leq e_0 \tag{1}$$

and

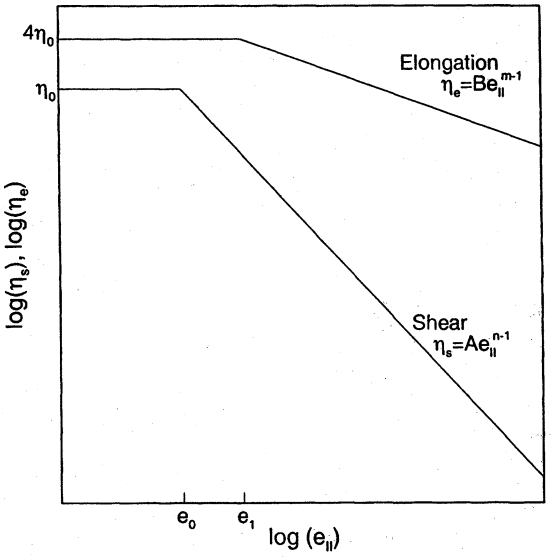

Figure 1. *Truncated power-law model for shear and elongational viscosities.*

$$\eta_e = Be_{II}^{m-1} \text{ for } e_{II} > e_1 \qquad \eta_e = 4\eta_0 \text{ for } e_{II} \leq e_1 \tag{2}$$

where $e_{II} = \sqrt{2(\tilde{e}:\tilde{e})}$ is the second invariant of the strain-rate tensor, η_s and η_e are the shear and elongational viscosities, respectively, and A and B are the consistency coefficients. The power-law indices (m, n) as well as the strain rates characterizing the transition from Newtonian to power-law behavior (e_0, e_1) can be different for the shear and elongational viscosities. As mentioned in Reference [22], the truncated power law model can accurately represent the elongational viscosity of many polymers such as HDPE [23,24] and polystyrene [25] and has been selected in the presented work because of its simplicity, and feasibility of separating the effects of elongational viscosity parameters m and e_1 on polymeric flows. However, our software can be used with any other equation specifying the strain-rate dependence of shear and elongational viscosities. It is noted that for $m = n$ and $e_0 = e_1$, the model given by Equations (1) and (2) is identical to a purely viscous generalized Newtonian formulation for a truncated power-law model with power-law index and Newtonian limit of n and e_0, respectively. The effects of elongational power-law index (m), Newtonian limit for elongational viscosity (e_1) and that of flow rate on entrance flow are analyzed in the next section. This paper only addresses the effect of steady-state elongational viscosity on entrance flow. The effects of the normal stress difference and transient behavior of elongational viscosity, which can also affect the vortices and extra pressure loss in entrance flow, have not been accounted in this work.

ENTRANCE FLOW

Following the terminology used in Reference [22], in this paper the entrance loss is expressed in terms of an equivalent length of the downstream channel:

$$L_e = \frac{\Delta p - \Delta p_1 - \Delta p_2}{\partial p_2} \tag{3}$$

where Δp is the total pressure drop in an entrance flow, Δp_1 and Δp_2 are, respectively, the pressure drop for fully developed flow in the portions of the channel upstream and downstream of the abrupt contraction, and ∂p_2 is the magnitude of the fully developed axial pressure gradient in the downstream channel. Trouton ratio ($Tr \equiv \eta_e / \eta_s$) for the strain rate at the downstream wall has been used in this paper to characterize the entrance flow.

By separately calculating the pressure drop due to shear and elongational flow near an abrupt contraction, Cogswell [29] developed analytical expressions for an approximate calculation of entrance loss for a fluid with different power-law indices for shear and elongational viscosities. Cogswell's expressions for entrance loss were further refined by Binding [30], who employed energy principle to relate the entrance loss and vortex length in an entrance flow to the flow rate and the shear and elongational viscosities of the polymer. Similar to the approach followed in this paper, Binding also used independent power-law models to represent the shear and elongational viscosities. Later in this section, for a planar 4:1 entrance flow, the extra pressure loss and vortex length predicted by a finite element simulation employing truncated power-law models for shear and elongational viscosities are compared with the corresponding values computed by using the analytical expressions developed by Binding [30]. It should be noted that the finite element predictions are expected to be somewhat different from the values calculated by Binding's analytical method because the power-law models are not truncated at low strain rates in Binding's analysis. Furthermore, Binding's analysis involves several simplifying assumptions, whereas, in the present work, strain-rate-dependence of shear and elongational viscosities has been captured in a frame-invariant constitutive equation. In particular, assuming a slow growth in the height of the recirculating vortex (h), that is, a large vortex, Binding neglected the terms involving $(dh/dx)^2$ and d^2h/dx^2 in the shear strain rate. However, for most of the entrance flow simulations reported later in this paper, $|dh/dx|$ for the recirculating vortex is greater than 1.

In Reference [22], for an axisymmetric 4:1 entrance flow, convergence of the numerical simulation was verified by using three successively refined meshes. Using the same finite element meshes, convergence of the numerical simulation of a planar 4:1 entrance flow has also been verified. The most refined of the three meshes (mesh C in Reference [22]) has been used for all the finite element simula-

tions reported in this paper. Unless specified otherwise, length of upstream and downstream channels is $20h_2$ and $30h_2$ respectively, where h_2 is the half-height of the downstream channel. Using the symmetry of the problem, only the flow on one side of the axis is simulated. Along with the no-slip boundary condition at the wall and symmetry condition on the axis, a fully developed flow has been specified at the entrance and the exit.

Effect of Elongational Power-Law Index on Entrance Flow

If the Newtonian limits for the shear and elongational viscosities and the power-law index for the shear viscosity are fixed, then for any strain rate beyond the Newtonian limits, the Trouton ratio increases as the elongational power-law index is increased. Therefore, keeping the flow rate and all other viscosity parameters fixed, as the elongational power-law index is increased, the extra pressure loss and recirculating vortex in an entrance flow are expected to grow. With the flow rate, Newtonian limits for the shear and elongational viscosities, and power-law index for shear viscosity being constant ($n = 0.25$, $e_0 = e_1 = 0.001\ s^{-1}$, $\dot{\gamma}_{av} = U / h_2 = 1\ s^{-1}$, where U and $\dot{\gamma}_{av}$ are, respectively, the average velocity and strain rate in the downstream channel), Figure 2 shows the effect of elongational power-law index (m) on the recirculating vortex in a planar 4:1 entrance flow. To depict the flow direction, Figure 2 shows the unit vectors along the direction of velocity. For $m = 0.25$, which corresponds to a purely viscous generalized Newtonian formulation for the truncated power-law model with $n = 0.25$ and $e_0 = 0.001\ s^{-1}$, in Figure 2(a) a small recirculating vortex is formed near the abrupt contraction. As the elongational power-law index is increased to $m = 0.4$ [Figure 2(b)], the recirculating vortex grows significantly. At $m = 0.47$ [Figure 2(c)], a lip vortex is also formed near the entrant corner. For the planar 4:1 entrance flow, lip vortex is formed only for a narrow range of elongational power-law index ($m = 0.46 - 0.48$) and it always seems to overlap with the corner vortex. In contrast, for an axisymmetric 4:1 entrance flow, a much larger lip vortex was observed in Reference [22]. These numerical predictions agree with the experimental observations of Walters and coworkers. Based upon their experimental work, Walters et al. [1,3,6,7] concluded that in comparison to the axisymmetric case, formation of lip vortex is rare in a planar entrance flow. A large recirculating vortex with the center of circulation close to the entrant corner is formed for $m = 0.5$ [Figure 2(d)]. As the elongational power-law index is increased beyond 0.5, [see Figure 2(e) for $m = 0.7$] the recirculating vortex continues to grow and the center of circulation moves away from the entrant corner. For $n = 0.25$, $e_0 = e_1 = 0.001\ s^{-1}$ and $\dot{\gamma}_{av} = 1\ s^{-1}$, the planar 4:1 entrance flow simulation converged up to $m = 0.7$, which corresponds to $Tr = 200.6$ (see Appendix). As mentioned in Reference [22], even though the numerical simulation never diverged, for extremely large Trouton ratio, elongational stresses due to computational error in velocity field start to

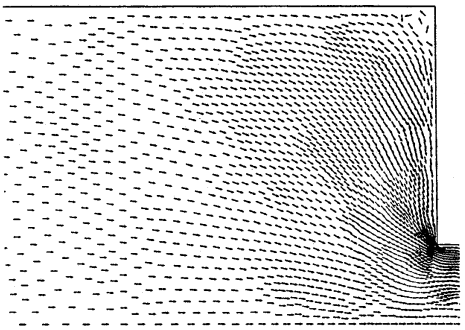

(a)

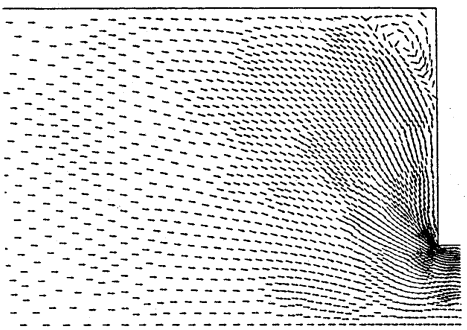

(b)

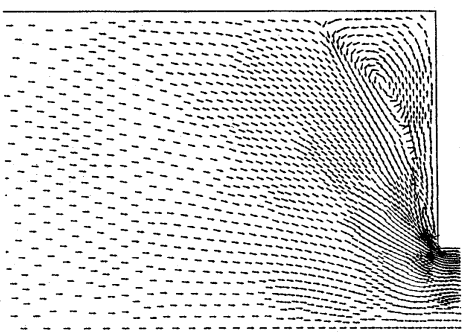

(c)

Figure 2. *Recirculation in 4:1 abrupt contraction for* n = *0.25,* $e_0 = e_1 = 0.001\ s^{-1}$ *and* $\dot{\gamma}_{av} = 1s^{-1}$. *The elongational power-law index,* m, *is (a) 0.25, (b) 0.4, (c) 0.47, (d) 0.5 and (e) 0.7.*

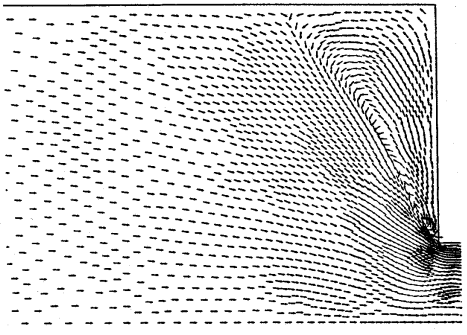

(d)

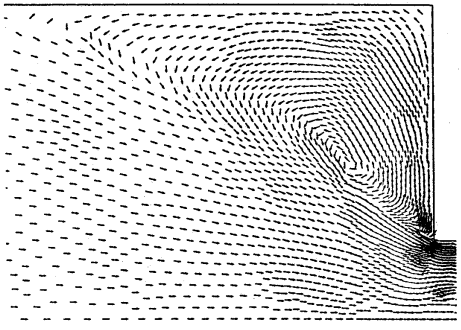

(e)

Figure 2 (continued). *Recirculation in 4:1 abrupt contraction for* n = 0.25, $e_0 = e_1 = 0.001\ s^{-1}$ *and* $\dot{\gamma}_{av} = 1 s^{-1}$. *The elongational power-law index,* m, *is (a) 0.25, (b) 0.4, (c) 0.47, (d) 0.5 and (e) 0.7.*

dominate the shear stresses and the simulations fails to converge to a specific value even for flow in a channel without a contraction.

For $n = 0.25$, $e_0 = e_1 = 0.001\ s^{-1}$ and $\dot{\gamma}_{av} = 1\ s^{-1}$, Figure 3 shows the effect of elongational power-law index on the velocity along the center line. For axisymmetric 4:1 entrance flow in Reference [22], near the abrupt contraction, 0.56% overshoot was observed in the center-line velocity for $m = 0.25$. In Figure 3, for $m = 0.25$, which corresponds to the truncated power-law model for a purely viscous generalized Newtonian fluid, no such overshoot is found in the centerline velocity for a planar 4:1 entrance flow. For $m > 0.25$, near the abrupt contraction, which is located at $x/h_2 = 0$ in Figure 3, a kink (without any overshoot) is observed in the centre-line velocity. As the elongational power-law index is increased, this kink in the center-line velocity occurs at a lower normalized velocity and a longer distance is required to reach the fully developed velocity profile.

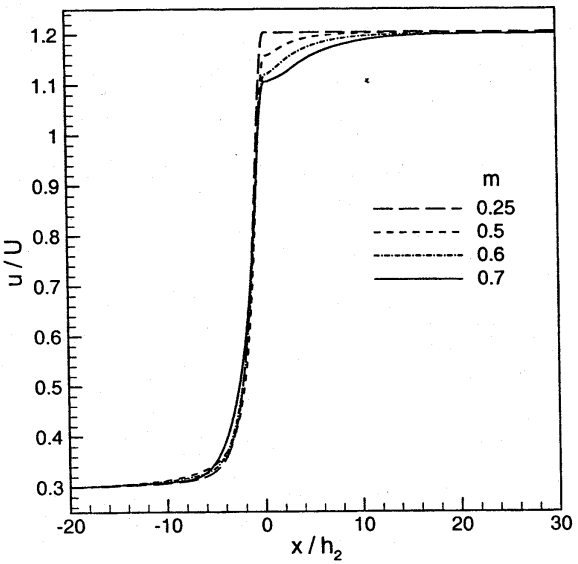

Figure 3. *Velocity along the axis of symmetry for* $n = 0.25$, $e_0 = e_1 = 0.001\ s^{-1}$, $\dot{\gamma}_{av} = 1 s^{-1}$ *and various values of the elongational power-law index.*

For various values of elongational power-law index, Figure 4 shows the normalized pressure variation along the center line, where the normalization has been performed with respect to the shear stress at the wall in the downstream channel. The effect of elongational power-law index on entrance loss, which corresponds to the steep drop in the center-line pressure near the abrupt contraction in Figure 4, is shown in Figure 5. For $m = 0.25$, the predicted entrance losses in terms of the equivalent length of the downstream channel L_e are, respectively, 1.8 and 1.42 for planar and axisymmetric cases, which are in good agreement with the values of entrance loss reported in the literature [8–12] for 4:1 entrance flow of a purely viscous power-law fluid with $n = 0.25$. The entrance loss increases rapidly as the elongational power-law index is increased. Interestingly, at higher values of m, for the axisymmetric and planar cases, entrance pressure loss in terms of the equivalent lengths of the downstream channel are almost the same. For instance, for $m = 0.7$, the equivalent lengths for the axisymmetric and planar cases are 20.97 and 20.7, respectively. Figure 5 also shows the entrance loss computed by using Binding's approximate analysis [30]. In view of various simplifying assumptions in Binding's analysis and the difference in the rheological models at low strain rates, the agreement between the entrance loss predicted by Binding's analytical method and that by finite element flow simulation is quite good. However, the vortex length (L_v) calculated by Binding's approximate method is much larger than the

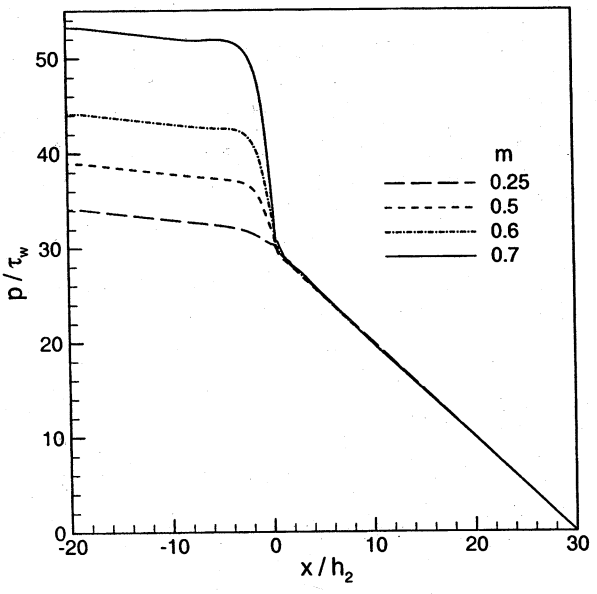

Figure 4. *Pressure along the axis of symmetry for* n = *0.25,* $e_0 = e_1 = 0.001\ s^{-1}$, $\dot{\gamma}_{av} = 1 s^{-1}$ *and various values of the elongational power-law index.*

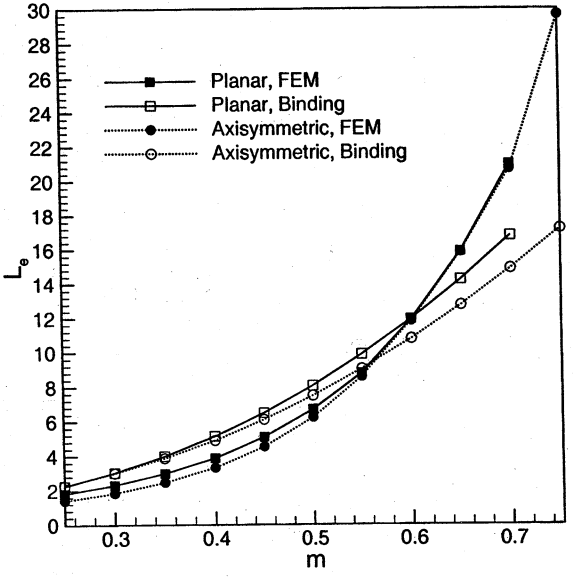

Figure 5. *Entrance loss vs.* m *for* n = *0.25,* $e_0 = e_1 = 0.001\ s^{-1}$ *and* $\dot{\gamma}_{av} = 1 s^{-1}$.

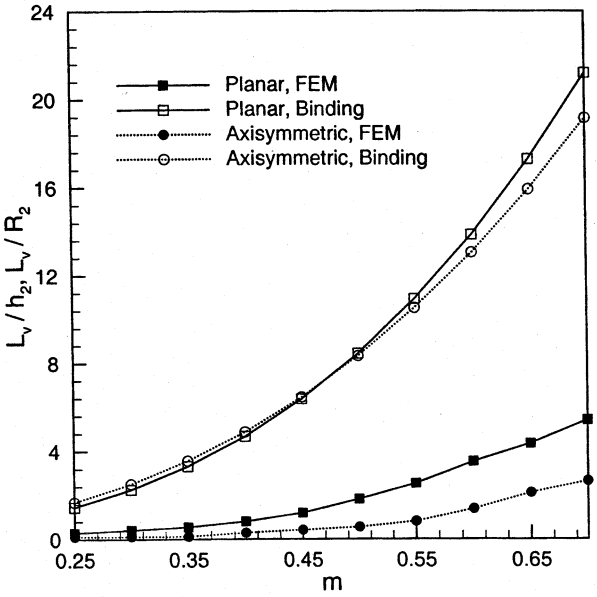

Figure 6. *Vortex length vs.* m *for* n = *0.25,* $e_0 = e_1 = 0.001\ s^{-1}$ *and* $\dot{\gamma}_{av} = 1 s^{-1}$.

corresponding predictions from the finite element simulation (Figure 6). As mentioned for axisymmetric entrance flow in Reference [22] in Figure 6 the vortex length from finite element simulation is the axial distance between the abrupt contraction and the farthest node with a positive velocity component in the upstream direction. Even though away from the recirculating vortex the velocity and pressure fields have converged with respect to the mesh refinement, depending upon the location of nodes in the mesh, the vortex length was found to change as much as 10% as the finite element mesh was refined successively. Therefore, the finite element prediction of the vortex length reported in this paper may have an error as large as ±10%. However, the discrepancy between the vortex length predicted by the finite element simulation and that by Binding's analysis is much beyond this error in the finite element predictions. Such a disagreement between the two estimates of the vortex length is not completely unexpected because the vortex length in Binding's analysis is actually the length of the upstream channel over which the flow is not fully developed, which is generally much larger than the vortex length. In Figure 6, Binding's approximate method predicts similar vortex lengths in the axisymmetric and planar entrance flows, whereas, the vortex length predicted by finite element simulation of the planar entrance flow is larger than the corresponding prediction for the axisymmetric case. It is noted that in comparison with axisymmetric flow, the experimental results [1,2,6] reported in the literature have

found a weaker vortex enhancement for planar entrance flow. Even though these observations seem to contradict the numerical predictions in Figure 6, since the axisymmetric and planar elongational viscosities of a polymer can be different, a weaker vortex enhancement in planar entrance flow is certainly feasible, if the power-law index for the planar elongational viscosity is higher than that for the axisymmetric elongational viscosity.

Effect of Newtonian Limits

Keeping the flow rate, Newtonian limit for the shear viscosity (e_0) and the shear and elongational power-law indices (n,m) fixed, if the Newtonian limit for elongational viscosity (e_1) is increased, the value of Trouton ratio increases for all strain rates beyond e_1. Therefore, for fixed power-law indices at a constant flow rate, the extra pressure loss and recirculating vortices in an entrance flow are expected to grow with e_1. It should be noted that a change in e_1 also affects the value of B in Equation (2).

With the flow rate and all other viscosity parameters fixed ($\dot{\gamma}_{av} = 1\ s^{-1}$, $n = 0.25$, $m = 0.5$, $e_0 = 0.001\ s^{-1}$), effect of e_1 on the extra pressure loss for 4:1 entrance flow is shown in Figure 7. For $e_1 > 0.02\ s^{-1}$, the simulation does not converge. Since Trouton ratio increases as e_1 is increased, the entrance loss in Figure 7 in-

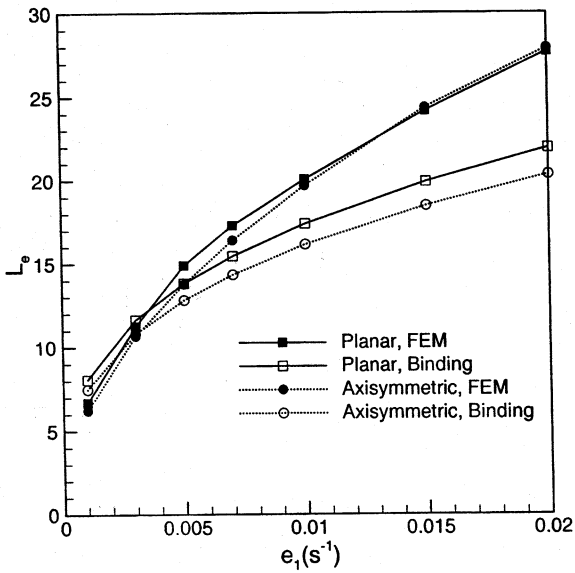

Figure 7. *Entrance loss vs.* e_1 *for* $n = 0.25$, $m = 0.5$, $e_0 = 0.001\ s^{-1}$ *and* $\dot{\gamma}_{av} = 1 s^{-1}$.

creases rapidly with e_1. At higher values of Trouton ratio, that is, large e_1, in terms of the equivalent length of the downstream channel, entrance losses predicted by finite element simulation of axisymmetric and planar entrance flows are almost the same. The entrance loss calculated by using Binding's approximate analysis, which is also shown in Figure 7, is in reasonable agreement with the predictions from the finite element flow simulation. Binding's method predicts a slightly lower entrance loss for the axisymmetric case.

For planar 4:1 entrance flow, Figure 8 shows the change in the vortex length as the elongational Newtonian limit is increased. The variation in vortex length in Figure 8 follows the same trends as those observed in Figure 6. In particular, the vortex length calculated from Binding's method, which is actually the length of the upstream channel over which the flow is not fully developed, is much larger than the vortex length predicted by the finite element flow simulation. Binding's method predicts almost the same vortex length for the axisymmetric and planar cases, whereas the vortex length predicted by finite element simulation is larger for the planar entrance flow. For $e_1 = 0.015\ s^{-1}$, the vortex length predicted by finite element simulation is slightly smaller than the vortex length for $e_1 = 0.01\ s^{-1}$. As mentioned in the last section, even though the flow field away from the recirculating vortex has converged with respect to the mesh refinement, vortex length predicted by finite element simulation may have an error of $\pm 10\%$. The fluctuation in Figure 11 is within the accuracy of the predicted vortex length.

Effect of Flow Rate

If all the parameters for the shear and elongational viscosities are fixed and the power-law index for elongational viscosity is larger than the index for the shear viscosity, then for $e_{II} > e_1$, the value of Trouton ratio increases with strain rate. Therefore, the extra pressure loss and recirculating vortex in a planar 4:1 entrance flow are expected to grow as the flow rate is increased. For constant values of shear and elongational viscosity parameters ($n = 0.25, m = 0.5, e_0 = e_1 = 0.001\ s^{-1}$), the effect of flow rate on entrance loss in a planar 4:1 entrance flow is shown in Figure 9. The simulation does not converge as the flow rate is increased beyond $\dot{\gamma}_{av} = 1000\ s^{-1}$. The simulation indicates that the entrance loss increases rapidly as the flow rate is increased. Figure 10 shows the variation in vortex length as the flow rate is increased. The variations in entrance loss and vortex length in Figures 9 and 10, respectively, follow the same trends as those observed in Figures 5–8. In particular, the entrance loss predicted by Binding's approximate analysis, which is also shown in Figure 9, is in reasonable agreement with the corresponding predictions from the finite element flow simulation. In comparison to the vortex length predicted by finite element flow simulation (Figure 10), Binding's analysis predicts a much larger vortex length.

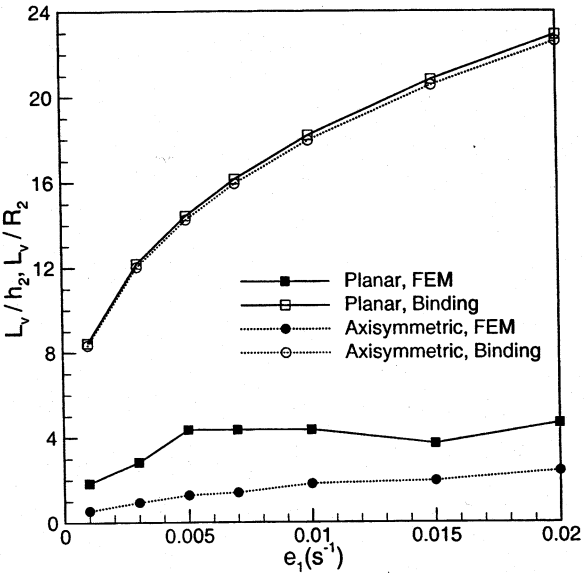

Figure 8. *Vortex length vs.* e_1 *for* n = 0.25, m = 0.5, $e_0 = 0.001\ s^{-1}$ *and* $\dot{\gamma}_{av} = 1 s^{-1}$.

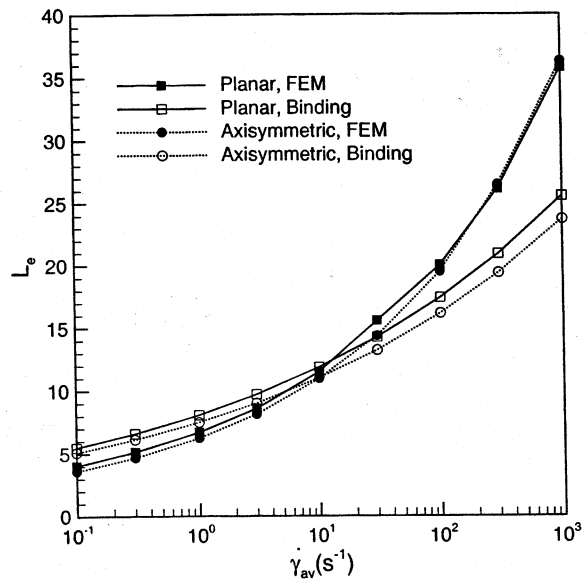

Figure 9. *Entrance loss vs.* $\dot{\gamma}_{av}$ *for* n = 0.25, m = 0.5 *and* $e_0 = e_1 = 0.001\ s^{-1}$.

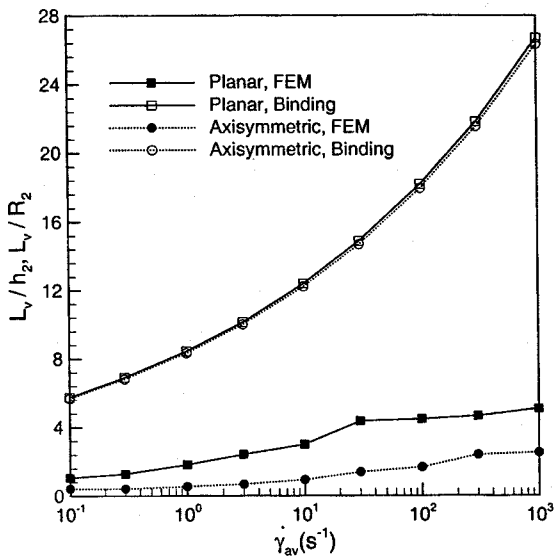

Figure 10. *Vortex length vs.* $\dot{\gamma}_{av}$ *for* n = *0.25,* m = *0.5 and* $e_0 = e_1 = 0.001\ s^{-1}$.

APPENDIX

Value of Trouton ratio at the downstream channel wall in a 4:1 abrupt contraction:

(a) For $n = 0.25$, $e_0 = e_1 = 0.001\ s^{-1}$, $\dot{\gamma}_{av} = 1\ s^{-1}$

m	0.25	0.35	0.45	0.55	0.65	0.7
Tr	4.0	9.5	22.8	54.4	129.8	200.6

(b) For $n = 0.25$, $m = 0.5$, $e_0 = 0.001\ s^{-1}$, $\dot{\gamma}_{av} = 1\ s^{-1}$

$e_1(s^{-1})$	0.001	0.003	0.005	0.01	0.02
Tr	35.2	61.0	78.7	111.3	157.4

(c) For $n = 0.25$, $m = 0.5$, $e_0 = e_1 = 0.001\ s^{-1}$,

$\dot{\gamma}_{av}(s^{-1})$	0.1	1	10	100	1000
Tr	19.8	35.2	62.6	111.3	198.0

REFERENCES

1. K. Walters and M. F. Webster, *Philos. Trans. R. Soc. London A,* 308, 199 (1982).
2. K. Walters and D. M. Rawlinson, *Rheol. Acta,* 21, 547 (1982).
3. R. E. Evan and K. Walters, *J. Non-Newtonian Fluid Mech.,* 20, 11 (1986).
4. D. V. Boger, *Annu. Rev. Fluid Mech.,* 19, 157 (1987).
5. S. A. White, A. D. Gotsis and D. G. Baird, *J. Non-Newtonian Fluid Mech.,* 24, 121 (1987).
6. D. M. Binding and K. Walters, *J. Non-Newtonian Fluid Mech.,* 30, 233 (1988).
7. R. E. Evan and K. Walters, *J. Non-Newtonian Fluid Mech.,* 32, 95 (1989).
8. D. V. Boger, R. Gupta and R. I. Tanner, *J. Non-Newt. Fluid Mech.,* 4, 239 (1978).
9. M. E. Kim-E, R. A. Brown and R. C. Armstrong, *J. Non-Newt. Fluid Mech.,* 13, 341 (1983).
10. E. Mitsoulis, J. Vlachopoulos and F. A. Mirza, *Polym. Eng. Sci.,* 24, 707 (1984).
11. C. A. Hieber, *Rheol. Acta,* 26, 92 (1987).
12. M. Gupta, C. A. Hieber and K. K. Wang, *Polym. Eng. Sci.,* 34, 209 (1994).
13. R. Keunings, Chapter 9 in *Fundamentals of Computer Modelling for Polymer Processing,* C. L. Tucker (ed.), Hanser, Munich (1989).
14. B. Debbaut, J. M. Marchal and M. J. Crochet, *J. Non-Newtonian Fluid Mech.,* 29, 119 (1988).
15. D. Rajagopalan, R. C. Armstrong and R. A. Brown, *J. Non-Newtonian Fluid Mech.,* 36, 159 (1990).
16. A. Bolch, P. Townsend and M. F. Webster, *J. Non-Newtonian Fluid Mech.,* 54, 285 (1994).
17. R. Guenette and M. Fortin, *J. Non-Newtonian Fluid Mech.,* 60, 27 (1995).
18. B. Purnode and M. J. Crochet, *J. Non-Newtonian Fluid Mech.,* 65, 269 (1996).
19. M. Gupta, C. A. Hieber and K. K. Wang, *Int. J. Numer. Meth. Fluids,* 24, 493 (1997).
20. C. Beraudo, A. Fortin, T. Coupez, Y. Demay, B. Vergnes and J. F. Aggasant, *J. Non-Newtonian Fluid Mech.,* 75, 1 (1998).
21. S. C. Xue, N. Phan-Thein and R. I. Tanner, *J. Non-Newtonian Fluid Mech.,* 74, 195 (1998).
22. M. Gupta, *Polym. Eng. Sci.,* 40, 23 (2000).
23. H. M. Luan, in *Rheology,* Vol. 2, G. Astarita, G. Marrucci and L. Nicolais (eds.), Plenum, New York 419–424 (1980).
24. H. Munstedt and H. M. Luan, *Rheol. Acta,* 20, 211 (1981).
25. J. A. van Aken and H. Janeschitz-Kriegl, *Rheol. Acta,* 19, 744 (1980); 21, 388 (1982).
26. J. F. Stevenson, *AICHE J.,* 18, 540 (1972).
27. H. M. Luan and H. Schuch, *J. Rheol.,* 33, 119 (1989).
28. N. E. Hudson and J. Ferguson, *Trans. Soc. Rheol.,* 20, 265 (1976).
29. F. N. Cogswell, *Polym. Eng. Sci.,* 12, 64 (1972).
30. D. M. Binding, *J. of Non-Newtonian Fluid Mech.,* 27, 173 (1988).